Composite Structures 175 (2017) 46–57

Contents lists available at ScienceDirect

Composite Structures

journal homepage: www.elsevier.com/locate/compstruct

Bending behavior of sandwich composite structures with tunable 3D-printed core materials

Tiantian Li, Lifeng Wang *

Department of Mechanical Engineering, State University of New York at Stony Brook, Stony Brook, NY 11794, USA

ARTICLE INFO

Article history:
Received 27 February 2017
Revised 18 April 2017
Accepted 2 May 2017
Available online 4 May 2017

Keywords:
Sandwich structure
Composites
Negative Poisson's ratio
Honeycombs
Mechanical property

ABSTRACT

We combine 3D printing technique, numerical analysis, and experiments to design a new class of sandwich composites that exhibit various bending behaviors. These programmed sandwich structures contain 3D printed core materials with truss, conventional honeycomb, and re-entrant honeycomb topologies. Three-point bending tests are performed to investigate the bending behavior of these sandwich composites with two types of carbon fiber reinforced polymer face sheets. Under bending deformation, sandwich composites with truss core materials provide highest flexural stiffness and strength that are desirable in structural components. The sandwich composites with re-entrant honeycomb core exhibit a sequential snap-through instability which significantly enhances the energy absorption abilities. Our experimental and numerical results indicate that architected core structures can be utilized to tailor the bending properties as well as failure mechanisms. These findings offer new insights into the study of nonlinear mechanical response of sandwich structures, which can benefit a wide range of industries and applications.

1. Introduction

Sandwich composite structures are widely used in aerospace, naval, sporting and automotive applications due to their high stiffness/weight ratio, high strength/weight ratio, and energy absorption capacity [1]. Typical sandwich structures consist of two thin, stiff and strong face sheets separated by a lightweight core that is usually made of polymeric foam, honeycomb or corrugated core etc. The core material keeps the face sheets in their relative positions in the sandwich with little increase in weight, to increase bending and buckling resistance [2,3], as well as shear stiffness and energy absorption ability [4]. The mechanical behavior of a sandwich composite depends on the material used for construction, geometry of face sheets and especially the core topology design. Among all sandwich core materials, foams core has been firstly studied [5] while they exhibit poor scaling due to their bending-dominated architecture [6]. Compared with the random porous structures of foams, various ordered cellular architectures with improved mechanical properties are applied to sandwich core configurations. The most widely studied and used one is conventional honeycomb cellular core [7–10]. Many analytical, numerical, and experimental investigations have suggested that sandwich structures with conventional honeycomb cellular core are stiff, strong, light and absorb much energy when crushed especially in out-of-plane direction [3,11–14]. Another attractive sandwich core is lattice truss materials [15–17]. Recent researchers have proposed that the textile truss cores are superior to regular honeycomb because of their superior buckling resistance at low relative density [18–22], and these open-celled counterparts would not trap moisture and possess multifunctional capabilities [15].

More recently, auxetic structures have received considerable attention because they exhibit unusual properties of becoming thicker when stretched; that is, they have negative Poisson's ratios. Due to the auxetic effects, auxetic cellular materials have many engineering advantages, such as increased indentation resistance [23], shear resistance [24], plane strain fracture toughness [25–27], and energy absorption [28–31]. Furthermore, auxetic structures exhibit synclastic bending [32–36], and have better acoustic properties compared to their conventional counterparts [37]. Based on the classical continuum theory, the auxeticity of materials can enhance certain mechanical properties, such as less deflection during bending [28] and increased shear modulus [24], making the structures ideal for use as sandwich core topology. Among various auxetic materials and structures discovered, re-entrant honeycomb has been investigated frequently by many researchers. The analytical studies on the re-entrant honeycomb

* Corresponding author.
E-mail address: lifeng.wang@stonybrook.edu (L. Wang).

http://dx.doi.org/10.1016/j.compstruct.2017.05.001
0263-8223/

have been reported on their mechanical properties under small deformation [3,38–42] and large deformation [43,44]. Moreover, it has been theoretically shown that the re-entrant honeycomb has enhanced shear properties compared to conventional materials [45,46]. Hou et al. [47,48] have studied the bending and failure of sandwich structures with auxetic gradient honeycomb cores. Imbalzano et al. [49,50] have numerically studied the performance of impact resistance for the sandwich panels with auxetic lattice cores. Yang et al. [51] have designed a sandwich structure with a 3D re-entrant auxetic core fabricated using electron beam melting and selective laser sintering and bending behavior on these materials has been studied. However, systematical studies on bending behavior of sandwich structures with auxetic core topology in comparison with non-auxetic core topology have not been largely explored. Conventionally, auxetic structures have been fabricated through multiple steps where the control of the specific geometry is quite difficult. Recently 3D printing, also known as additive manufacturing, has been developed rapidly, which enables the fabrication of auxetic cellular materials with precise and complex cellular geometries directly from the CAD models [52].

In the present study, re-entrant honeycomb, conventional honeycomb, and truss cellular structures are designed using CAD software and then fabricated using 3D printing technique. Uniaxial compression tests are conducted to investigate the Poisson's ratios of these three designs as compared with theoretical prediction. Three-point bending tests are performed to obtain the mechanical properties, including bending stiffness, strength, and energy absorption of the sandwich composites consisting these three designed core materials. Two types of face sheets are selected: unidirectional carbon fiber reinforced polymer (U-CFRP) and woven carbon fiber reinforced polymer (W-CFRP). A finite element analysis (FEA) is further carried out to compare the stress distributions in these sandwich composites. Moreover, different failure mechanisms are explored and indicate their potentials in structural applications.

2. Materials and methods

2.1. Structural design

The geometric features of the proposed sandwich core design of truss, conventional honeycomb, and re-entrant honeycomb are discussed here. Fig. 1 illustrates the schematic of three lattice microstructures. The relative density for each configuration can be calculated as

For truss

$$\frac{\rho^*}{\rho_S} = \frac{t}{L\sin\theta\cos\theta} \tag{1}$$

For conventional and re-entrant honeycombs

$$\frac{\rho^*}{\rho_S} = \frac{t/L(H/L+2)}{2\cos\theta(H/L+\sin\theta)} \tag{2}$$

Here the relative densities as 0.2, 0.3 and 0.4 are considered. Therefore, the thickness of cell walls can be calculated from the Eqs. (1) and (2), respectively. Three types of cellular structures are fixed to have the same dimension of the unit cell, as 9 mm × 9 mm. Details of the parameters for each design are listed in Table 1. Under small deformation, the in-plane Poisson's ratio can be evaluated [3] asFor truss

$$\upsilon_{12} = \cot\theta \tag{3}$$

For conventional and re-entrant honeycombs

$$\upsilon_{12} = \frac{\cos^2\theta}{(H/L+\sin\theta)\sin\theta}. \tag{4}$$

For re-entrant honeycomb, θ is negative, then the Poisson's ratio of the cell becomes negative in values. Therefore, according to the Eqs. (3) and (4), the Poisson's ratio of truss, conventional honeycomb, and re-entrant honeycomb in current design are evaluated as 1, 1.732 and −1.732, respectively. Here, the re-entrant honeycombs are orthotropic and they also have a Poisson's ratio, υ_{21}. However, we specifically focus on the Poisson's ratios, υ_{12}, in this work due to the compressive and tensile deformation induced by bending of the sandwich composites are both in the direction 1.

The sandwich beams are designed to have overall dimensions of 108 mm × 21 mm × 10 mm and be composed by 12 × 2 unit cells. Two thin layers are also added to the top and bottom of the core structures to improve the connection alignment with the sandwich face sheets. Fig. 2(a) shows a sandwich beam for bend test. The geometric parameters are listed in Table 2.

2.2. Sample preparation

The proposed sandwich core materials are fabricated using a 3D printer (Objet Connex260, Stratasys) and VeroWhite (VW, an acrylic-based photopolymer) is taken as the constitutive material for the core structures. Considering the anisotropic nature of 3D printing technology due to layer-by-layer fabrication process, the layer orientation is found to influence the mechanical properties of the material; therefore, all the specimens are printed along the same orientation. The as-fabricated specimens are kept at room temperature for 7 days to allow for the saturation of the curing.

Three types of sandwich specimens with VeroWhite, woven carbon fiber reinforced polymer and unidirectional carbon fiber reinforced polymer as the face sheets are made respectively. U-CFRP is directly ordered from Graphtek LLC. W-CFRP is fabricated in our lab, which is a 16 layers of carbon fiber ordered in $(0°/90°)_4^{sym}$, reinforced in Vinylester matrix. The fabrication process includes the cold-bonded of CFRP in vacuum. The material properties of VW, W-CFRP and U-CFRP are obtained by uniaxial tensile testing of each material following the ASTM D638 standard, as shown in Table 3. After all the core material and face sheets are completely manufactured, two face sheets are adhered to one core structure together by epoxy adhesive (E-00NS). All specimens are kept by attachment for one day to make sure they are bonded adhesively then dried for 7 days to allow coherent between the core and skins. After that, the surfaces of the sandwich skins are cleaned to avoid the effect of remaining glue on the bending test.

2.3. Mechanical testing

The compression test and three-point bending test are performed using a MTS mechanical tester (C43 frame) with a 10 kN load cell. The quasi-static compression is carried out at a constant strain rate of 0.005 s^{-1}. Three-point bending test is carried out at a loading rate of 0.008 mm/s and the span length is 72 mm (Fig. 2 (b)). Images of the specimens at various loading conditions are taken at a rate of 1 FPS (VicSnap, Correlated Solution).

2.4. Numerical simulation

The finite element analysis is conducted using commercial software ABAQUS (Dassault Systemes Simulia Corp., Providence, RI). Plane stress condition is assumed during the simulations. The models are meshed with 6-node triangular elements and 6 elements are generated along the width of the cell walls after a convergence test. The true stress-strain relation of VeroWhite observed from uniaxial tension is directly exported to ABAQUS and implemented as the constitutive equation for the core material. W-CFRP and U-CFRP are modeled as elastic-perfectly plastic

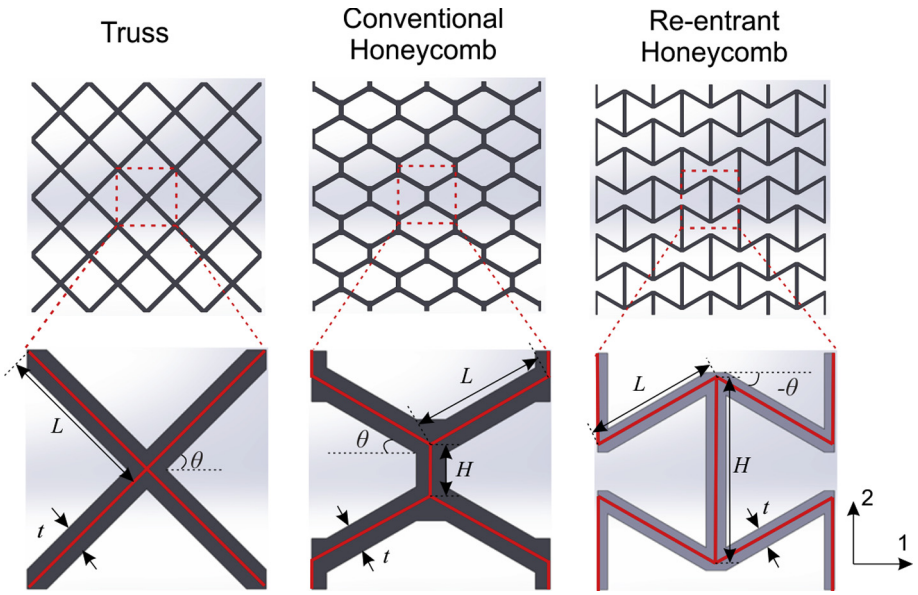

Fig. 1. Design of unit cell of the truss, conventional honeycomb, and re-entrant honeycomb structure. Here, L is the length of the inclined cell walls of truss structures; t is the thickness of the cell walls; and θ is the angle between the inclined cell walls. The shapes of regular and re-entrant honeycomb structures are described as the length of the vertical cell walls, H; the length of the inclined cell walls, L; the thickness of the cell walls, t, and the angle between the vertical and inclined cell walls, θ.

Table 1
Design parameters of truss, conventional honeycomb, and re-entrant honeycomb (Unit: mm).

	Truss			Conventional Honeycomb				Re-entrant Honeycomb			
ρ_c^*/ρ_S	L	t	θ	L	H	t	θ	L	H	t	θ
0.2	6.37	0.67	45°	5.2	1.9	0.71	30°	5.2	7.1	0.50	-30°
0.3	6.37	1.04	45°	5.2	1.9	1.11	30°	5.2	7.1	0.76	-30°
0.4	6.37	1.44	45°	5.2	1.9	1.56	30°	5.2	7.1	1.04	-30°

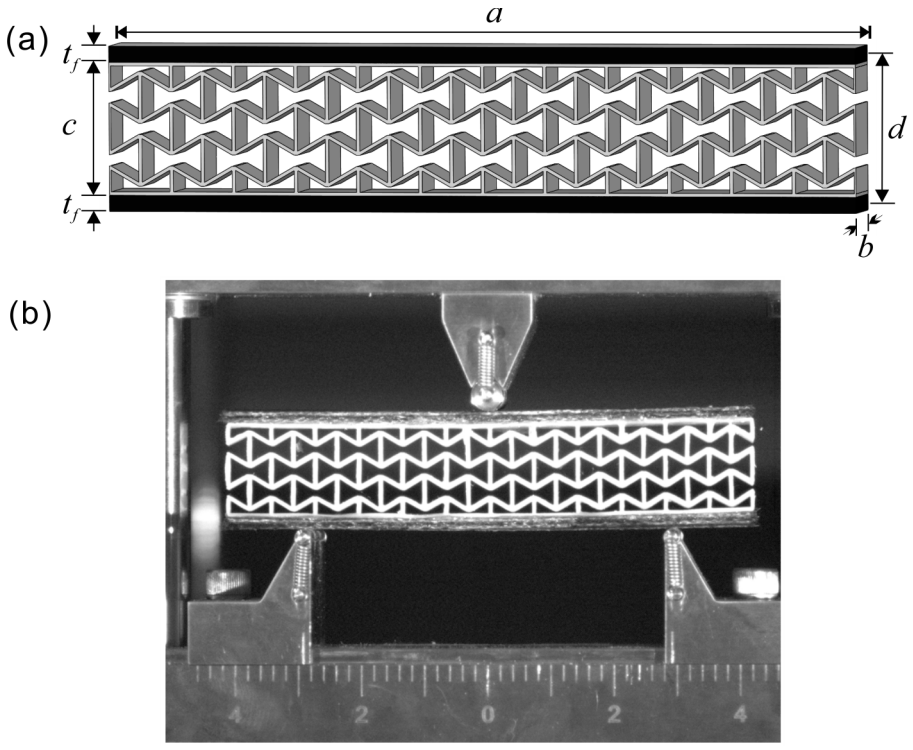

Fig. 2. (a) Sandwich structures for bending test. The subscript 'f' refers to the face sheets. Here, a is the length of the beam; b is the width; c is the core thickness; t_f is the face sheet thickness; d is the distance between centroids of faces. (b) Set-up of the three-point bending test.

Table 2
Design geometric parameters of sandwich composite structures for bending test (Unit: mm).

Core			Sandwich panel					
VeroWhite			VeroWhite		W-CFRP		U-CFRP	
a	b	c	t_f	d	t_f	d	t_f	d
108	10	19	1	20	2.3	21.3	1.5	20.5

Table 3
Material properties.

	VeroWhite	W-CFRP	U-CFRP
Young's modulus (GPa)	1.6	26	94 (longitudinal)
Yield Strength (MPa)	66	390	1400 (longitudinal)

materials. In addition, geometric nonlinearity is considered to represent the large deformation of the structure.

3. Results and discussion

3.1. Poisson's ratio of core design

Fig. 3 shows the mechanical response of re-entrant honeycomb, conventional honeycomb, and truss cellular specimens under uniaxial compression, respectively. The nominal stress-strain curves indicate these structures exhibit linear stress-strain relations up to 8% macroscopic strain. The Poisson's ratio for each specimens is determined in this linear-elastic deformation region. Fig. 3(c-e) shows the images of re-entrant honeycomb, conventional honeycomb and truss specimens under compression at $\varepsilon = 0$, -0.04, and -0.08, respectively. It is seen that the lateral boundaries of the re-entrant honeycomb sample shrink continuously under compression, indicating a negative Poisson's ratio of this material. While the conventional honeycomb and truss specimens exhibit lateral expansion during the uniaxial compression, which shows a positive Poisson's ratio. To quantify the deformation in the specimens during the experiments, an image processing software (ImageJ) is used to determine the position of intersection points in the specimens. Because the deformation near the four edges of the specimen is affected by boundary conditions, we focus on the behavior of unit cells in the central region of the specimens. The relations between the average horizontal strain and the average vertical strain of the unit cells are plotted in Fig. 3(b). The local values of Poisson's ratio can be calculated by estimating the slope of the horizontal strain and vertical strain curves. Over the linear elastic deformation region, the experimental determined Poisson's ratio is approximately a constant at $\nu_{12} = 1.070$ for truss, $\nu_{12} = 1.730$ for conventional honeycomb and $\nu_{12} = -1.732$ for re-entrant honeycomb, respectively, which shows an excellent agreement with the analytical estimates 1.000, 1.732 and -1.732, respectively. Here, for the purpose of ensuring a fair comparison, we design that the conventional honeycomb and the re-entrant honeycomb have the same absolute value of Poisson's ratio, ν_{12} .

3.2. Bending performance of sandwich composites

Having demonstrated that the re-entrant honeycomb lattice material exhibit auxetic behavior and conventional honeycomb and truss lattice material exhibit non-auxetic behavior under uniaxial compression, we now systematically investigate the bending behavior of the sandwich composite specimens with different cores and face sheets.

3.2.1. Effect of face sheets

Fig. 4(a) shows the load-deflection relations of the sandwich composite specimens with different face sheets: VW, W-CFRP, and U-CFRP. Here the core of sandwich specimens is a re-entrant honeycomb with a relative density of 0.2. It is clear that the face sheet material will affect the bending behavior significantly. As expected, the load-deflection relation of the sandwich specimen with VW face sheets shows the lowest force level because VW is softer and weaker than a CFRP. While for the sandwich specimen with W-CFRP face sheets, load significantly increases to the yield point ~190 N at 4 mm and maintains a plateau up to 20 mm before a complete failure. For the sandwich specimen with U-CFRP face sheets, the load-deflection curve exhibits the highest force level to a maximum of 500 N and two enhanced load stages are observed. Therefore, compared to W-CFRP, U-CFRP will significantly enhance the energy absorption behavior of the sandwich composite structures. These different mechanical responses are intrinsically controlled by the stiffness and strength of the face sheets, which is shown in Table 3. Another phenomenon could be noticed that for specimens with U-CFRP face sheets, the load-deflection curve indicates negative bending stiffness behavior due to the snap-through instabilities of the re-entrant core under loading and the details will be discussed later. The images of three sandwich specimens at a deflection of 15 mm are shown in Fig. 4(b). At the final stage of bending the sandwich specimen with VW face sheets shows less deformation in core ligaments while the sandwich specimen with U-CFRP face sheets exhibit the largest deformation in core ligaments. Therefore, the deformation mechanism of these sandwich composite structures with the same core material is strongly dominated by the mechanical properties of sandwich face sheets that are carrying loads by mainly tension/-compression during sandwich beam bending.

3.2.2. Effect of core topology

The effect of the core topology on the bending behavior are examined experimentally and numerically. Here we use U-CFRP as the face sheets and the relative density of sandwich cores is 0.2 for each core topology. Fig. 5(a) shows that the specific core topology has a significant impact on the load-deflection curves. The truss core sandwich composite structure has the largest flexural stiffness and maximum loading forces, while the re-entrant honeycomb core sandwich composite structure has the lowest flexural stiffness and largest bending deflection. It can be easily understood as the re-entrant honeycomb has much lower Young's modulus and stress lever at the same deformation lever, as seen in Fig. 3(a), as compared with the other two core structures, leading to weaker mechanical response of the re-entrant honeycomb sandwich composite structure. Fig. 5(b) shows the images of three sandwich specimens at a deflection of 8 mm. Core fractures occur in the truss and the conventional honeycomb sandwich composite structures, as also evident from the drops in the load-deflection curves, which indicates that these sandwich structures will fail locally. It is noticed that the shear of the core materials causes the failure of the truss and the conventional honeycomb sandwich composite structures. The shear resistance or shear strength of the core materials plays an important role during the bending of sandwich structures. Based on Gibson's model [3], we estimate the

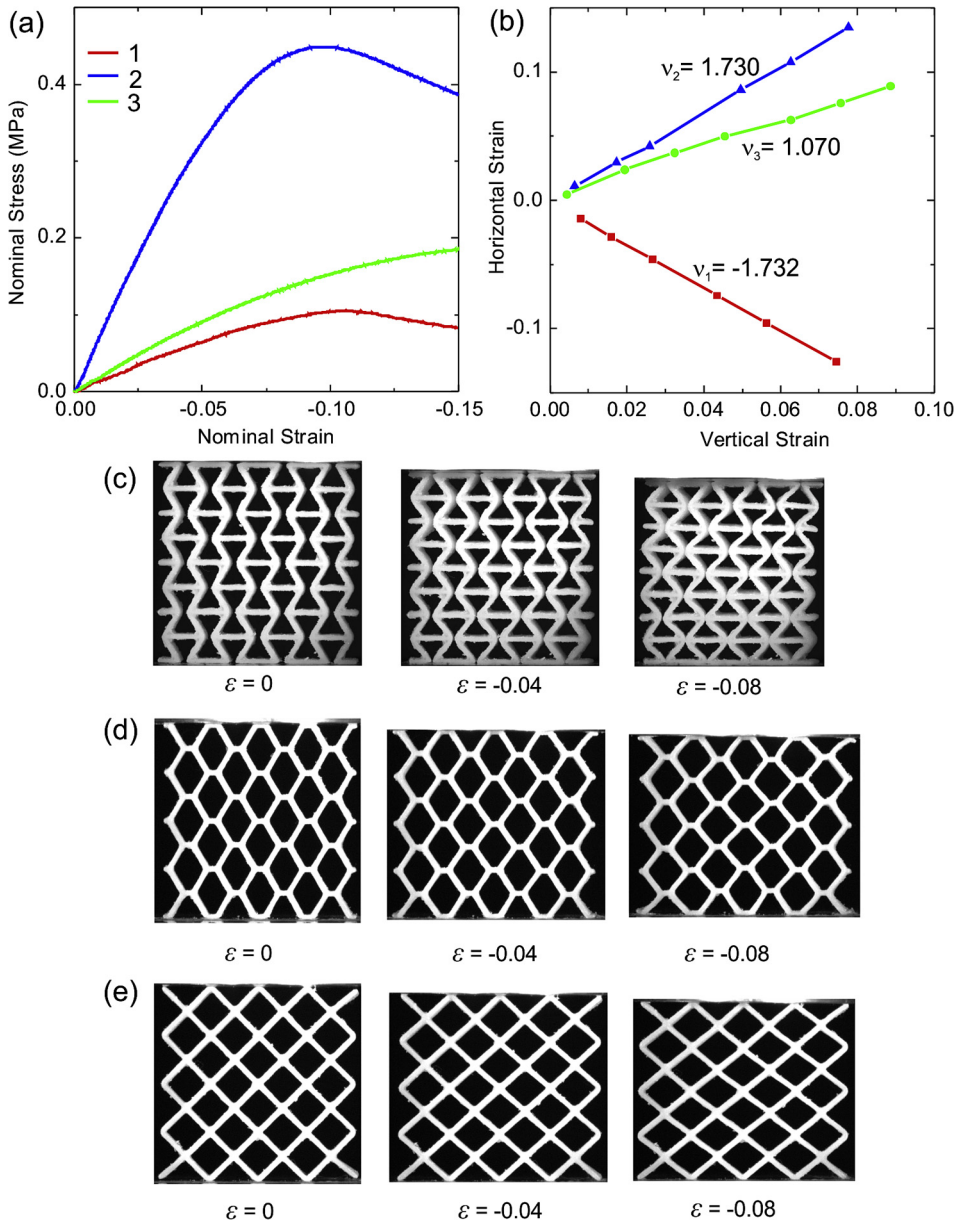

Fig. 3. Three cellular core materials under uniaxial compression test (the volume fraction is 20%): re-entrant honeycomb (Specimen 1), conventional honeycomb (Specimen 2), and truss (Specimen 3), respectively. (a) Nominal stress-strain curves; (b) The horizontal strain as a function of the vertical strain, where Poisson's ratio is calculated; (c-e) each specimen under compression at strains of $\varepsilon = 0$, $\varepsilon = -0.04$, and $\varepsilon = -0.08$.

shear strength of the conventional honeycomb as: $\frac{(\tau^*_{pl})_{12}}{\sigma_{ys}} = \frac{1}{4}\left(\frac{t}{L}\right)^2 \frac{1}{H/L\cos\theta}$, which reduces to $0.10548^*\left(\frac{t}{L}\right)^2$. For the shear strength of the truss, we estimate the shear strength as: $\frac{(\tau_{pl^*})_{12}}{\sigma_{ys}} = \frac{1}{8}\frac{t}{L}$. Using our design parameters, the estimation of the effective shear resistance of these core materials, $\frac{(\tau_{pl^*})_{12}}{\sigma_{ys}}$, is listed in Table 4. We could notice that the truss structures exhibit higher shear strength than that of the conventional honeycomb, which is consistent with the experiment results. Moreover, using the scaling law $\frac{(\tau_{pl^*})_{12}}{\sigma_{ys}} = C^*\left(\frac{\rho_S}{\rho^*_C}\right)^n$, we could calculate that the scaling exponent equals to 2.267 for the conventional honeycomb and 1.103 for the truss structure, which indicates that the deformation mechanism is bending-dominated for the conventional honeycomb and stretching-dominated for the truss structure. Interestingly, no fractures are observed in the re-entrant honeycomb sandwich composite structure up to a large deflection (16 mm in this case). Instead, buckling of ligaments is seen in each layer. The buckling phenomenon does not result in the catastrophic failure but the periodic re-entrant honeycomb structures contain the buckling deformation and enable the sandwich composite structure to provide energy absorption to a larger deformation. Therefore, global failure mode controls the re-entrant honeycomb sandwich composite structures. Furthermore, the core deformation in truss and conventional honeycomb sandwich specimens are irreversible after unloading due to fractures of ligaments. On the contrary, at the same level of global deformation for the re-entrant honeycomb sandwich specimen with low density (20%), the deformation of core structures is mostly buckling of ligaments instead of fractures, which provides the possibility for these types of sandwich composite structures with strong potentials of reusable abilities. Moreover, the 3D-printed material for fabricating the core structures is a glassy polymer with shape memory effect. It is possible to use the temperature for the shape recovery after the plastic defor-

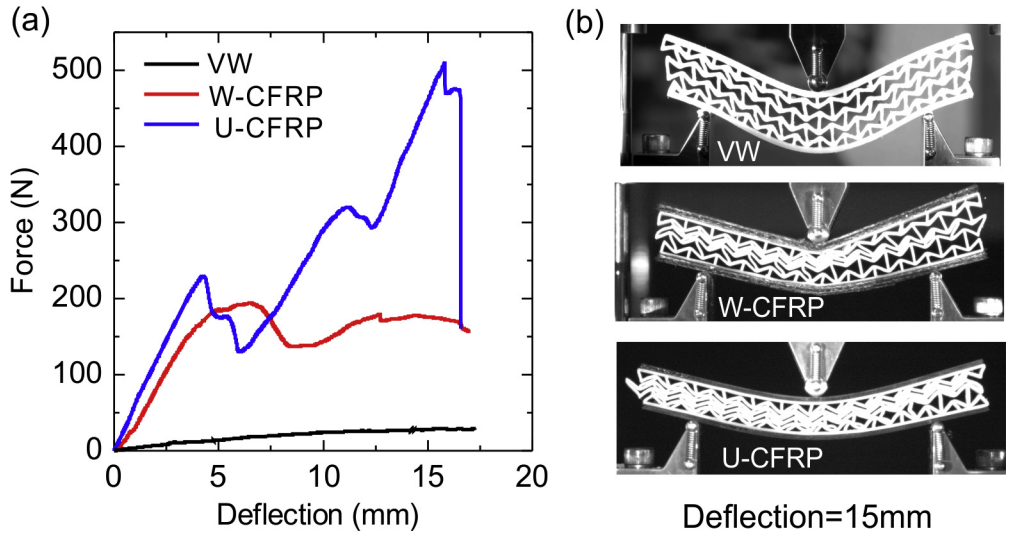

Fig. 4. Bending characteristic of sandwich composite specimens with face sheets of different materials. The core is re-entrant honeycomb with an effective density of 0.2. (a) Load-deflection curves; (b) the images of deformed configuration of each sandwich specimen at a deflection of 15 mm.

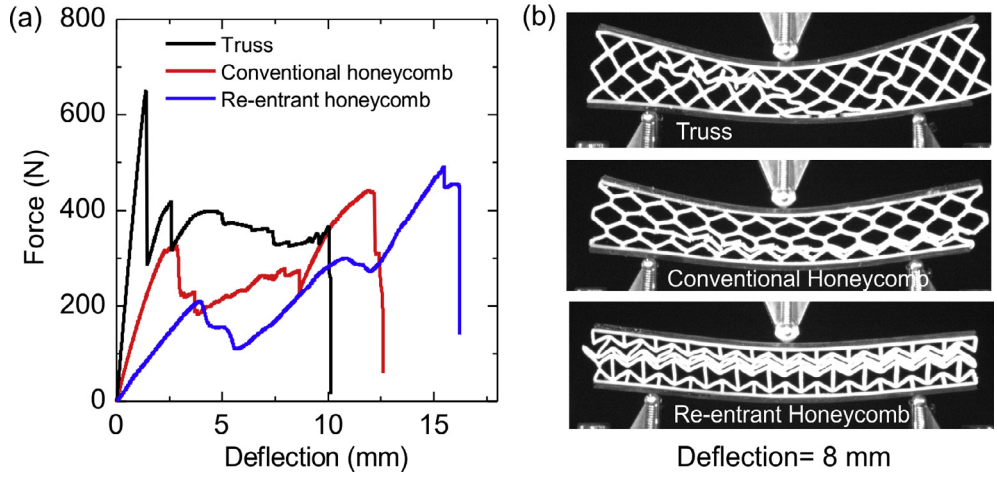

Fig. 5. Bending characteristic of sandwich composite specimens with different core structures and U-CFRP face sheets. The effective density of core material is 0.2 for all specimens. (a) Load-deflection curves; (b) the images of deformed configuration of each sandwich specimen at a deflection of 8 mm.

Table 4
The normalized shear strength of truss and conventional honeycomb with various relative densities.

Relative density	0.2	0.3	0.4
Truss	0.0131	0.0204	0.0282
Conventional honeycomb	0.00197	0.0048	0.0095

mation, which may lower the repair costs. For the re-entrant honeycomb sandwich specimen with core density higher than 0.2, it exhibits fractures of ligaments instead of the buckling due to the low slenderness ratio of the ligaments.

Fig. 6 shows the comparison of the experiments and FEA prediction, indicating good agreement between the numerical and experimental results. Excellent agreement can be observed in the force displacement curves between the numerical and experimental results at displacement up to the yield of the sandwich specimens, as shown in Fig. 6(a). As larger displacement, the experiments show failures of ligaments, leading to significant drops in the force displacement curves, which is not captured by the FEA simulation since no fracture criteria is taken into consideration in the simulations. Fig. 6(b) shows the deformed specimens in the experiments and Fig. 6(c) exhibits the corresponding specimens in the simulations. For re-entrant honeycomb sandwich composite structure, simulation confirms the buckling of vertical ligaments observed in the experimental test. Moreover, the simulated von Mises stresses show that re-entrant honeycomb sandwich composite structure exhibits relatively homogeneous stress distribution in both face sheets and core material. Especially the stress level in the ligaments is lower than those in the truss and conventional honeycomb cores. Therefore, local failure does not occur due to the less localized stress concentration. For conventional honeycomb and truss sandwich structures, it is apparent that the stress distribution is largely concentrated in the area near loading point and some certain struts where local failure would be expected. The results of the FEA simulation and the average experimental measurement calculated from Fig. 6(a) are listed in Table 5. Again, one can notice an excellent agreement on the flexural strength between the simulation and the experiment. The simulated flexural stiffness is slightly higher than the experimentally observed value, which is attributed to the base material constitutive behavior. Specifically, we use a stress-strain relation measured from uniaxial tension experiment

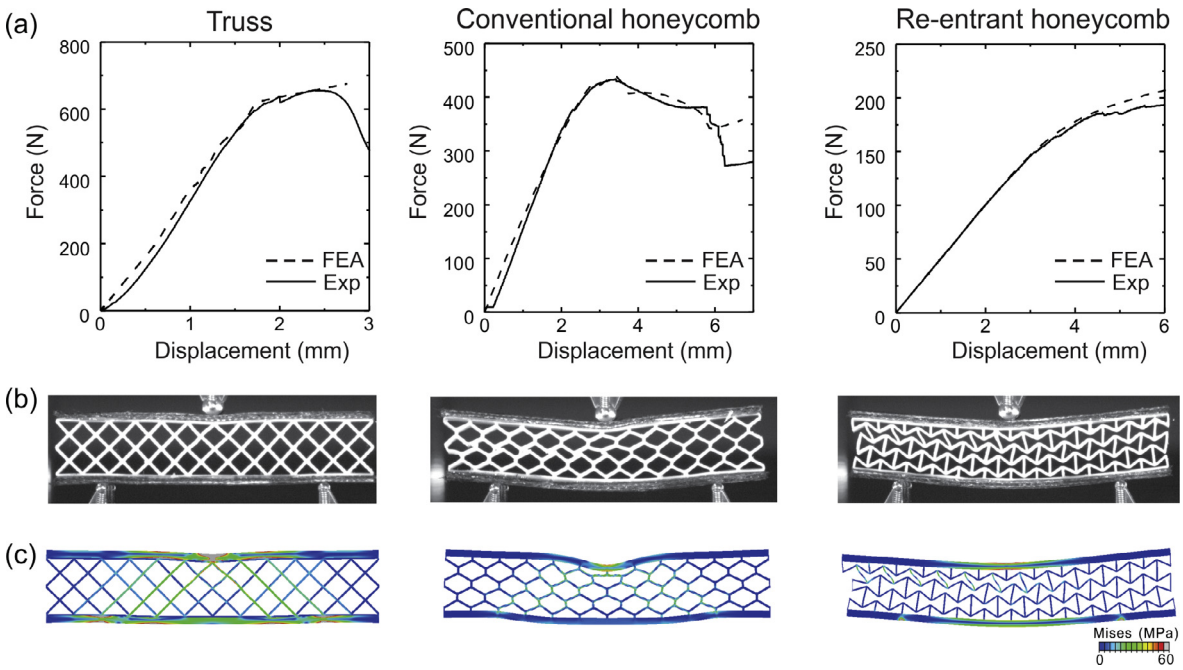

Fig. 6. Comparison of the experiments and FEA predications for mechanical response of sandwich composites under bending deformation. (a) The force-displacement curves. (b) The experimentally deformed specimens and (c) the corresponding simulated FEA results of the three sandwich composite structures with truss composite at a deflection of 1.5 mm, conventional honeycomb composite at a deflection of 2.5 mm, and re-entrant honeycomb composite at a deflection of 3.8 mm.

Table 5
Comparison of FEA and experimental results of the sandwich composite specimens with W-CFRP face sheets.

Core design	Measured Strength (MPa)	FEA simulated Strength (MPa)	Measured Modulus (GPa) (GPa)	FEA simulated Modulus (GPa)
Re-entrant honeycomb	3.76	3.98	35.74	35.61
Conventional honeycomb	8.39	8.31	109.65	136.48
Truss	12.72	12.94	292.98	343.39

of VW. However, during bending tests, the ligaments could be subjected to tension, compression, or bending. This complex stress state is not well captured in a simple elastic-plastic material model. Moreover, the fidelity of the 3D printed process will also affect the materials properties. Although Objet 260 has a stated resolution of ~16 μm, the accuracy can still affect the volume fraction and distribution of printed materials. Anisotropy, porosity, and imperfections introduced during 3D printing also play a role. These specific aspects are not taken into consideration in our model. Compared to conventional honeycomb and truss core, the re-entrant honeycomb sandwich composites exhibit relative low flexural strength and stiffness, therefore, a larger bending deflection could be expected. These results suggest good ability to tailor the core topology to achieve different bending behaviors for certain mechanical applications.

Fig. 7 shows the load-deflection curves and the corresponding images of deformed re-entrant honeycomb sandwich specimens at different level of deflections. Interestingly, the deformation process of the sandwich beams with re-entrant honeycomb core exhibit a snap-through instability during three-point bending tests. Three re-entrant honeycomb sandwich specimens with core relative density of 0.2 are tested and show good repeatability (Fig. 7 (a)). The load-deflection response is characterized by three peaks and drops; the first and second drops correspond to the sequential buckling of ligament layers and the third drop corresponds to the catastrophic failure of the whole structure, as shown in Fig. 7(b). During the bending, the vertical ligaments in the mid row of core structures will buckle first due to the core shear concentration during bending. The instability leads to a drop in the load-deflection curve, which makes the slope become negative, where negative incremental bending stiffness is observed. After the buckled vertical ligaments become in contact with the inclined ligaments in the middle row, the load increases again. The instability occurs through row-by-row, with simultaneously increasing the load level until the whole specimen is fully deflected. Furthermore, at larger deformation, the plasticity affects the behavior of instability for the re-entrant honeycomb sandwich structures [53]. The composite sandwich structure can absorb energy through bending plastic hinges which connect to two inclined ligaments and one vertical ligament. Because of the core shear, the vertical ligaments first buckle and then incline to one side with the rotation of neighboring plastic hinges leading to the resistance of these plastic hinges to the external force. With increasing bending deformation, the rotation of plastic hinges induces the contact of vertical ligaments and the inclined ligaments, which will ensure the structure to continue to carry more load.

The relative density of re-entrant honeycomb core is found to significantly affect the snap-through instability. For the core with relative density above 0.3, the instability behavior vanishes. With the increase of the relative density, the slenderness ratio of ligaments will increase, which will make the core structure more brittle. Therefore, continuous loading will lead to the local catastrophic failure instead of buckling and the resulting load-deflection curves drop dramatically. Also, the material of face sheets will affect this phenomenon which could be seen in Fig. 4. The stiffer and stronger face sheets will be more beneficial to the instability behaviors. For the sandwich beams with conventional honeycomb core and truss core, the instability phenomenon could not be observed during

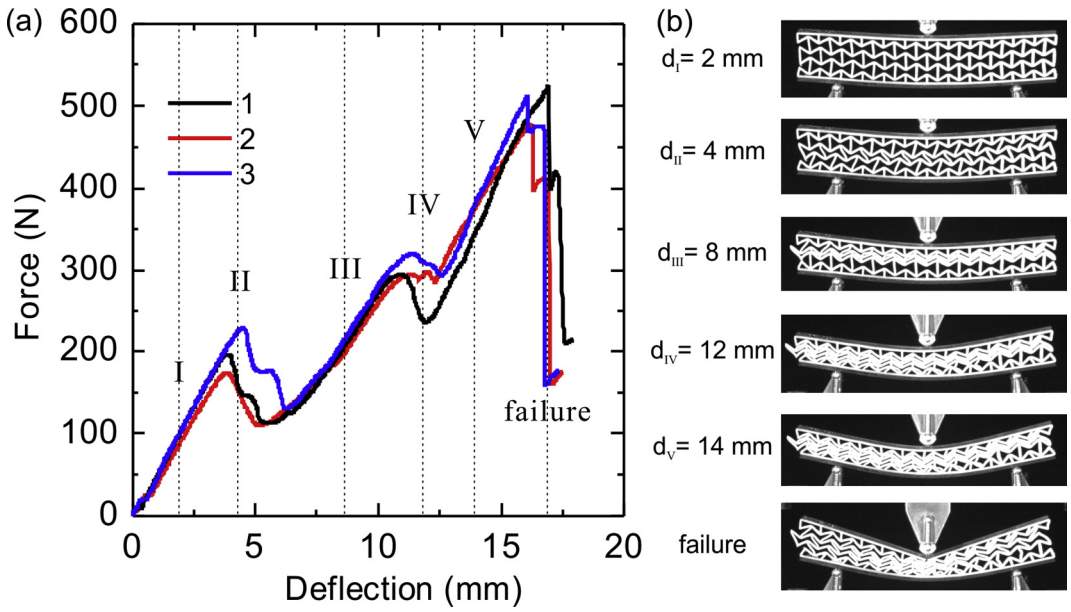

Fig. 7. Bending characteristic of sandwich composite specimens with re-entrant honeycomb core design and U-CFRP face sheets. Three specimens are used showing repeatability. The relative density of core material for each specimen is 0.2. (a) Load-deflection curves; (b) the images of deformed configuration of sandwich specimen 3 at different deflections.

three-point bending tests. Recently, the snap-through instabilities have been employed for material design in bi-stable periodic structures under compression [54–56] and tension [57]. The nonlinear mechanical response of these new classes of architected materials will significantly enhance the energy absorption ability whether via low rate quasi-static loading or via impact tests. Our sandwich structures with re-entrant honeycomb cores also exhibit the snap-through instability especially during the bending deformation. Note that, due to this deformation mechanism, the specific energy absorption of current sandwich structures is not as large as several recently developed architectured materials, such as hollow micro-truss structures [58], bicontinuous structures[59], buckyball [60] and honeytube structures [61], which are shown to exhibit significantly enhanced specific energy absorption. The combination of nonlinear deformation mechanism, the open-cell nature, as well as the tunability of the sandwich structures can provide better opportunities to integrate with new functionalities.

3.2.3. Effect of relative density

Fig. 8 depicts the experimental results of the maximum force, maximum deflection, flexural stiffness, and maximum energy absorption (which we compute as the work before catastrophic failure occurs) of sandwich composite structures with three core designs and relative density from 0.2 to 0.4. With increasing the relative density, the maximum force and flexural stiffness will increase significantly and the maximum deflection will decrease. This is as expected since sandwich composite structures with higher relative density of cores will become stiffer, stronger but brittle. At any given relative density of cores, the truss and conventional honeycomb sandwich composite structures provide a larger maximum force and a larger flexural stiffness than the re-entrant honeycomb sandwich composites. The re-entrant honeycomb sandwich composite structures possess a larger deflection and slightly smaller energy absorption. For many energy absorption applications, it is required that the structure exhibit a response force just below the injury criterion and a limited densification deflection [1]. Comparing the bending properties of three composite structures, we find that the re-entrant sandwich composites exhibit significant advantages over the truss or conventional honeycomb sandwich composites. The re-entrant honeycomb sandwich has the same level of energy absorption ability but with smaller response forces and much larger densification deflections compared to the truss and conventional honeycomb sandwiches. For example, for the sandwich composites with W-CFRP face sheets and relative density of 0.4, at the force level of 400 N, the re-entrant sandwich composites absorb about 100% energy (about 6 J) the same as the other two sandwich composites. While at the same energy absorption level, the conventional honeycomb and truss sandwich composite structures have a response force level around 800 N and 1300 N, respectively, which is significantly higher than those in the re-entrant honeycomb sandwich composite structure. Moreover, the failure mechanism of re-entrant honeycomb sandwich is global dominant, which provides less local deformation and failure. While the non-auxetic sandwiches' deformation are irreversible after failure because of the local fractures of cores. Therefore, the re-entrant honeycomb sandwich composites are better potential candidates for energy absorption applications. Meanwhile the truss sandwich composites and conventional honeycomb sandwich composites are ideal candidates for the applications where high specific stiffness and strength are required. These results suggest we could combine numerical calculation and 3D printing technique to tailor the microstructures of sandwich composites to achieve different bending properties for certain mechanical applications.

3.3. Discussion

We have shown that the flexural stiffness and flexural strength increase as the relative density of core material increases for the sandwich beams. Generally, for the cellular materials, such as metal foams and lattice structures, the relation between the effective elastic modulus E and the relative density ρ_C^*/ρ_S can be described by a power law $E = C(\rho_C^*/\rho_S)^n$ [3,62,63]. Therefore, these scaling laws could be used to describe the relation between the flexural stiffness and flexural strength and the relative density of cores for the sandwich composite structures. The flexural stiffness of sandwich composite structures [3,4] is calculated from the *equivalent flexural* rigidity, $(EI)_{eq}$, and the *equivalent shear rigidity*,

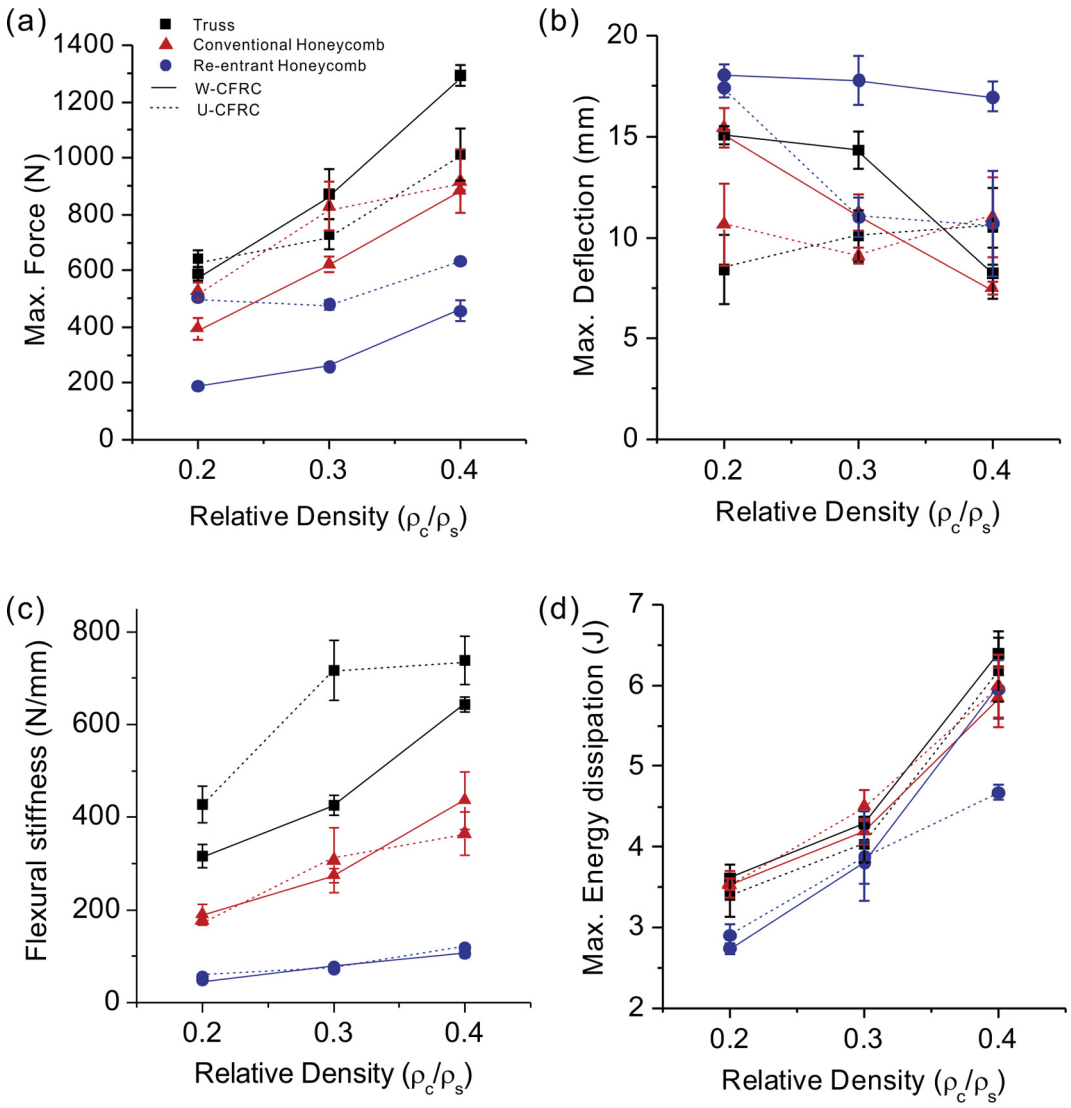

Fig. 8. Bending properties of the sandwich structures. (a-d) Maximum force, maximum deflection, flexural stiffness and maximum energy dissipation.

$(AG)_{eq}$, of the beam. Found from the parallel axis theorem, the equivalent flexural rigidity of the rectangular beam, as shown in Fig. 2(a), gives

$$(EI)_{eq} = \frac{E_f bt^3}{6} + \frac{E_c bc^3}{12} + \frac{E_f btd^2}{2}. \tag{5}$$

These three terms describe the bending stiffness of the faces, the bending stiffness of the faces and of the core about the centroid, and the bending stiffness of the faces about the centroid of the beam itself, respectively. In optimal sandwich design, the first two terms are small compared to the third term. As an approximation,

$$(EI)_{eq} = \frac{E_f btd^2}{2}. \tag{6}$$

The equivalent shear rigidity is

$$(AG)_{eq} = \frac{bd^2 G_C^*}{c}. \tag{7}$$

Here the shear modulus of the core, G_C^*, can be described as a function of solid polymer modulus, E_S, and the relative density of the core structure, ρ_C^*/ρ_S, via

$$G_C^* = C_1 E_S \left(\frac{\rho_C^*}{\rho_S}\right)^n \tag{8}$$

where C_1 and n can be obtained by fits to experimental data.

When the load, P, is applied, the deflection δ of the sandwich beam is the sum of the bending and shear components:

$$\delta = \delta_b + \delta_s = \frac{Pl^3}{48(EI)_{eq}} + \frac{Pl}{4(AG)_{eq}}. \tag{9}$$

Using Eqs. (6)–(9), the flexural stiffness of the sandwich beam is

$$\frac{P}{\delta} = \frac{4bd^2}{\frac{l^3}{6tE_f} + \frac{cl}{C_1 E_S}\left(\frac{\rho_S}{\rho_C^*}\right)^n}. \tag{10}$$

Furthermore, the failure modes of a sandwich beam include face yielding, face wrinkling, core failure, failure of the adhesive bond and core indentation. However, we notice the dominant failure mechanism of our sandwich specimens is the core shear. In this study, the face thickness to span ratio, t/l, are 0.014 for U-CFRP and 0.032 for W-CFRP. Our experimental results indicate that the face sheets do not fail, instead the core shears. If decreasing the thickness of the face sheets, the failure mode may transform from core shear to face yield, which will affect the deformation mode of

Table 6
The relations of the flexural stiffness and strength to the relative density of core designs for the sandwich composite structures.

Sandwich structures		Flexural stiffness FEA Strength		Flexural strength FEA Modulus	
Core	Face sheets	C_1	n	C_2	m
Re-entrant Honeycomb	W-CFRP	0.0126	1.17	0.0547	1.23
	U-CFRP	0.0128	1.08	0.1019	1.46
Conventional Honeycomb	W-CFRP	0.1209	2.00	0.1076	1.98
	U-CFRP	0.1526	1.93	0.1443	1.80
Truss	W-CFRP	0.0609	1.00	0.1491	1.13
	U-CFRP	0.0672	0.92	0.2231	1.08

the composite sandwich structures. In this way, the fractures of core materials will not happen and the total energy absorption of the re-entrant honeycomb will more rely on the strength of the face sheets. Moreover, the snap-through instability may disappear and the advantage of re-entrant honeycomb sandwich compared with the truss and conventional honeycomb sandwiches may not exist. On the other hand, while increasing the thickness of the face sheets, the strength and stiffness will increase which will keep the failure mode as core shear. In this case, the deformation mode and the capability of energy absorption of the re-entrant honeycomb sandwich structures will be well maintained. Moreover, the shear stresses in the composite material change rapidly between the core and the skin, the adhesive layer also takes some degree of shear force. For our sandwich composites, the adhesive bond between the two layers is strong so that no delamination or de-bonding is observed. The failure load [3], which is the maximum force during the three-point bending test, can be described as a function of the yield stress of solid polymer, σ_{ys} and the relative density of the core structure, ρ^*/ρ_S, via

$$P_{\max} = 2C_2 bc\sigma_{ys}\left(\frac{\rho_C^*}{\rho_S}\right)^m \tag{11}$$

where C_2 and m can be obtained by fits to experimental data.

For sandwich composite beams with truss, conventional honeycomb, and re-entrant honeycomb cores, these parameters are given in Table 6. The scaling exponent n equal to 1 indicates stretch-dominated deformation behavior of the ligaments whereas an exponent of 2 typically indicates bending-dominated deformation. For the flexural stiffness, the power indexes n for the re-entrant honeycomb sandwich and the truss sandwich are around 1, so that the bending deformation for these two types of sandwich structures are almost stretch-dominated. In contrast, the power indexes n for the conventional honeycomb sandwich structures are around 2, indicating the contribution from the bending of the interconnected ligaments. Furthermore, for the flexural strength, the power indexes m are 1.98 and 1.80 for the conventional honeycomb sandwich and 1.13 and 1.08 for the truss sandwich. Compared with the scaling law of shear strength for the honeycomb and truss structures in Table 4, the power index from the model is 2.267 for honeycomb and 1.103 for truss, respectively, which shows a good agreement with experiment results. Moreover, the power indexes m for the re-entrant honeycomb sandwich are 1.23 and 1.46 which are larger than the n fitted from flexural stiffness. This is because the snap-through instability behavior appears in the sandwich structures with low relative density cores. For the conventional honeycomb and the truss honeycomb sandwich structures, the power indexes of the flexural stiffness and flexural strength are almost identical for each structure which means the flexural stiffness and flexural strength are mostly determined by the deformation mechanism resulting from the topology of sandwich cores.

In practical applications, the sandwich composites are increasingly considered to be used in aircrafts, marine structures, portable structures, special vehicles, and some sport equipment. For example, there is a wide range of naval structures being developed using fiber reinforced polymer composites, including patrol boats built completely of composites, super structures, decks, and masts in frigates and destroyer and even internal equipment and fittings [64]. These sandwich composites are usually exposed to severe static and dynamic loads which are related to the penetrating/impact loading. Therefore, we investigate the mechanical behaviors under three-point bending test instead of four-point bending test with consideration of penetration resistance. Recently, 3D porous architectures composed of a continuous surface including the triply periodic minimal surfaces [65–67] exhibit enhanced strength and stiffness at relative low density and they can also serve as potential core materials for sandwich composites with better mechanical performance. Interestingly, additional fillers, such as sand, polymer foam, liquid, and silicon rubber [68–71] in the cellular structures can decrease the stress concentration and enhance the stiffness, strength and energy absorption of the cellular structures in the sandwich structures. Future work will explore more geometrical and topological structures to combine the deformation of co-continuous phases to achieve higher mechanical performance.

4. Conclusion

We have manufactured a novel class of sandwich composite structures with 3D-printed core materials and CFRP face sheets. Truss, conventional honeycomb, and re-entrant honeycomb are designed as the core material topologies. Under uniaxial compression, the truss and conventional honeycomb structures provide a non-auxetic behavior while the re-entrant honeycomb structure provides an auxetic behavior as expected. The evaluated Poisson's ratio for each structure consists well with the theoretical prediction. Three-point bending tests are conducted and the flexural stiffness, flexural strength, and energy absorption are evaluated on these sandwich composite structures. Our experimental and numerical results show a very good agreement in terms of the deformation pattern, flexural stiffness, and flexural strength. Under bending, the re-entrant honeycomb sandwich structures show an interesting global failure mode because of the relatively homogeneous stress distribution. Moreover, the re-entrant honeycomb sandwich structures exhibit sequential snap-through instabilities which significantly increases the energy absorption capacity. In contrast, the truss and conventional honeycomb sandwich structures show catastrophic failure earlier due to the localized stress concentration. The findings presented here provide new insights into the development of sandwich composite structures with unique mechanical properties for a wide range of mechanical and structural applications.

Acknowledgements

The authors gratefully acknowledge the financial support from the National Science Foundation (CMMI-1437449, CMMI-

1462270) and the Office of Naval Research. The authors thank Prof. Fu-Pen Chiang (Stony Brook University) for his encouragement of this work.

References

[1] Schaedler TA, Carter WB. Architected cellular materials. Annu Rev Mater Res 2016;46:187–210.
[2] Zenkert D, Nordisk I. The handbook of sandwich construction. Cradley heath. West Midlands: Engineering Materials Advisory Services Ltd. (EMAS); 1997.
[3] Gibson LJ, Ashby MF. Cellular solids: structure and properties. Cambridge University Press; 1999.
[4] Allen HG. Analysis and design of structural sandwich panels: the commonwealth and international library: structures and solid body mechanics division. Elsevier; 2013.
[5] Triantafillou TC, Gibson LJ. Failure mode maps for foam core sandwich beams. Mater Sci Eng 1987;95:37–53.
[6] Ashby MF. Metal foams: a design guide. Boston: Butterworth-Heinemann; 2000.
[7] Burton WS, Noor AK. Assessment of continuum models for sandwich panel honeycomb cores. Comput Methods Appl Mech Eng 1997;145:341–60.
[8] Rathbun HJ, Radford DD, Xue Z, He MY, Yang J, Deshpande V, et al. Performance of metallic honeycomb-core sandwich beams under shock loading. Int J Solids Struct 2006;43:1746–63.
[9] Petras A, Sutcliffe MPF. Failure mode maps for honeycomb sandwich panels. Compos Struct 1999;44:237–52.
[10] Buitrago BL, Santiuste C, Sánchez-Sáez S, Barbero E, Navarro C. Modelling of composite sandwich structures with honeycomb core subjected to high-velocity impact. Compos Struct 2010;92:2090–6.
[11] Masters IG, Evans KE. Models for the elastic deformation of honeycombs. Compos Struct 1996;35:403–22.
[12] Becker W. Closed-form analysis of the thickness effect of regular honeycomb core material. Compos Struct 2000;48:67–70.
[13] Meraghni F, Desrumaux F, Benzeggagh ML. Mechanical behaviour of cellular core for structural sandwich panels. Compos A Appl Sci Manuf 1999;30:767–79.
[14] Hu H, Belouettar S, Daya EM, Potier-Ferry M. Evaluation of kinematic formulations for viscoelastically damped sandwich beam modeling. J Sandwich Struct Mater 2006;8:477–95.
[15] Sypeck DJ. Cellular truss core sandwich structures. Appl Compos Mater 2005;12:229–46.
[16] Sypeck DJ, Wadley HNG. Cellular metal truss core sandwich structures. Adv Eng Mater 2002;4:759–64.
[17] Hu Y, Li W, An X, Fan H. Fabrication and mechanical behaviors of corrugated lattice truss composite sandwich panels. Compos Sci Technol 2016;125:114–22.
[18] Wadley H. Fabrication and structural performance of periodic cellular metal sandwich structures. Compos Sci Technol 2003;63:2331–43.
[19] Fleck NA, Sridhar I. End compression of sandwich columns. Compos A Appl Sci Manuf 2002;33:353–9.
[20] Cote F, Biagi R, Bart-Smith H, Deshpande VS. Structural response of pyramidal core sandwich columns. Int J Solids Struct 2007;44:3533–56.
[21] Xiong J, Ma L, Pan S, Wu L, Papadopoulos J, Vaziri A. Shear and bending performance of carbon fiber composite sandwich panels with pyramidal truss cores. Acta Mater 2012;60:1455–66.
[22] George T, Deshpande VS, Wadley HNG. Mechanical response of carbon fiber composite sandwich panels with pyramidal truss cores. Compos A Appl Sci Manuf 2013;47:31–40.
[23] Lakes RS, Elms K. Indentability of conventional and negative poisson's ratio foams. J Compos Mater 1993;27:1193–202.
[24] Lakes R. Foam structures with a negative Poisson's ratio. Science 1987;235:1038–40.
[25] Yang W, Li Z-M, Shi W, Xie B-H, Yang M-B. Review on auxetic materials. J Mater Sci 2004;39:3269–79.
[26] Grima JN, Evans KE. Auxetic behavior from rotating squares. J Mater Sci Lett 2000;19:1563–5.
[27] Choi JB, Lakes RS. Fracture toughness of re-entrant foam materials with a negative Poisson's ratio: experiment and analysis. Int J Fract 1996;80:73–83.
[28] Evans KE. Auxetic polymers: a new range of materials. Endeavour 1991;15:170–4.
[29] Alderson A, Alderson KL. Auxetic materials. Proc Inst Mech Eng Part G: J Aerosp Eng 2007;221:565–75.
[30] Mohsenizadeh S, Alipour R, Shokri Rad M, Farokhi Nejad A, Ahmad Z. Crashworthiness assessment of auxetic foam-filled tube under quasi-static axial loading. Mater Des 2015;88:258–68.
[31] Hou S, Liu T, Zhang Z, Han X, Li Q. How does negative Poisson's ratio of foam filler affect crashworthiness? Mater Des 2015;82:247–59.
[32] Whitty JPM, Alderson A, Myler P, Kandola B. Towards the design of sandwich panel composites with enhanced mechanical and thermal properties by variation of the in-plane Poisson's ratios. Compos A Appl Sci Manuf 2003;34:525–34.
[33] Scarpa F, Ciffo LG, Yates JR. Dynamic properties of high structural integrity auxetic open cell foam. Smart Mater Struct 2004;13:49–56.
[34] Evans KE, Alderson A. Auxetic materials: functional materials and structures from lateral thinking! Adv Mater 2000;12:617–28.
[35] Evans KE, Alderson KL. Auxetic materials: the positive side of being negative. Eng Sci Educ J 2000;9:148–54.
[36] Alderson A, Alderson KL, Chirima G, Ravirala N, Zied KM. The in-plane linear elastic constants and out-of-plane bending of 3-coordinated ligament and cylinder-ligament honeycombs. Compos Sci Technol 2010;70:1034–41.
[37] Chen CP, Lakes RS. Micromechanical analysis of dynamic behavior of conventional and negative Poisson's ratio foams. J Eng Mater Technol 1996;118:285–8.
[38] Lee J, Choi JB, Choi K. Application of homogenization FEM analysis to regular and re-entrant honeycomb structures. J Mater Sci 1996;31:4105–10.
[39] Yang DU, Lee S, Huang FY. Geometric effects on micropolar elastic honeycomb structure with negative Poisson's ratio using the finite element method. Finite Elem Anal Des 2003;39:187–205.
[40] Gonella S, Ruzzene M. Homogenization and equivalent in-plane properties of two-dimensional periodic lattices. Int J Solids Struct 2008;45:2897–915.
[41] Assidi M, Ganghoffer J-F. Composites with auxetic inclusions showing both an auxetic behavior and enhancement of their mechanical properties. Compos Struct 2012;94:2373–82.
[42] Yang S, Qi C, Wang D, Gao R, Hu H, Shu J. A comparative study of ballistic resistance of sandwich panels with aluminum foam and auxetic honeycomb cores. Adv Mech Eng 2013;5.
[43] Wan H, Ohtaki H, Kotosaka S, Hu G. A study of negative Poisson's ratios in auxetic honeycombs based on a large deflection model. Eur J Mech A Solids 2004;23:95–106.
[44] Fu MH, Xu OT, Hu LL, Yu TX. Nonlinear shear modulus of re-entrant hexagonal honeycombs under large deformation. Int J Solids Struct 2016;80:284–96.
[45] Scarpa F, Tomlinson G. Theoretical characteristics of the vibration of sandwich plates with in-plane negative Poisson's ratio values. J Sound Vib 2000;230:45–67.
[46] Lira C, Scarpa F. Transverse shear stiffness of thickness gradient honeycombs. Compos Sci Technol 2010;70:930–6.
[47] Hou Y, Neville R, Scarpa F, Remillat C, Gu B, Ruzzene M. Graded conventional-auxetic Kirigami sandwich structures: Flatwise compression and edgewise loading. Compos B Eng 2014;59:33–42.
[48] Hou Y, Tai YH, Lira C, Scarpa F, Yates JR, Gu B. The bending and failure of sandwich structures with auxetic gradient cellular cores. Compos A Appl Sci Manuf 2013;49:119–31.
[49] Imbalzano G, Tran P, Ngo TD, Lee PV. Three-dimensional modelling of auxetic sandwich panels for localised impact resistance. J Sandwich Struct Mater 2015;1099636215618539.
[50] Imbalzano G, Tran P, Ngo TD, Lee PV. A numerical study of auxetic composite panels under blast loadings. Compos Struct 2016;135:339–52.
[51] Yang L, Harrysson O, West H, Cormier D. A comparison of bending properties for cellular core sandwich panels. Mater Sci Appl 2013;04(08). 7.
[52] Vogiatzis P, Chen S, Wang X, Li T, Wang L. Topology optimization of multi-material negative Poisson's ratio metamaterials using a reconciled level set method. Comput Aided Des 2017;83:15–32.
[53] Zhou Z, Zhou J, Fan H. Plastic analyses of thin-walled steel honeycombs with re-entrant deformation style. Mater Sci Eng, A 2017;688:123–33.
[54] Prasad J, Diaz AR. Synthesis of bistable periodic structures using topology optimization and a genetic algorithm. J Mech Des 2005;128:1298–306.
[55] Correa DM, Klatt T, Cortes S, Haberman M, Kovar D, Seepersad C. Negative stiffness honeycombs for recoverable shock isolation. Rapid Prototyping J 2015;21:193–200.
[56] Shan S, Kang SH, Raney JR, Wang P, Fang L, Candido F, et al. Multistable architected materials for trapping elastic strain energy. Adv Mater 2015;27:4296–301.
[57] Rafsanjani A, Akbarzadeh A, Pasini D. Snapping mechanical metamaterials under tension. Adv Mater 2015;27:5931–5.
[58] Liu Y, Schaedler TA, Chen X. Dynamic energy absorption characteristics of hollow microlattice structures. Mech Mater 2014;77:1–13.
[59] Lee JH, Wang LF, Boyce MC, Thomas EL. Periodic bicontinuous composites for high specific energy absorption. Nano Lett 2012;12:4392–6.
[60] Xu J, Li Y, Xiang Y, Chen X. Energy absorption ability of buckyball C(720) at low impact speed: a numerical study based on molecular dynamics. Nanoscale Res Lett 2013;8:54.
[61] Yin S, Li J, Liu B, Meng K, Huan Y, Nutt SR, et al. Honeytubes: hollow lattice truss reinforced honeycombs for crushing protection. Compos Struct 2017;160:1147–54.
[62] Ashby MF. The properties of foams and lattices. Philos Trans R Soc A: Math Phys Eng Sci 2006;364:15–30.
[63] Liu Y, Schaedler TA, Jacobsen AJ, Chen X. Quasi-static energy absorption of hollow microlattice structures. Compos B Eng 2014;67:39–49.
[64] Mouritz A, Gellert E, Burchill P, Challis K. Review of advanced composite structures for naval ships and submarines. Compos Struct 2001;53:21–42.
[65] Han SC, Lee JW, Kang K. A new type of low density material: shellular. Adv Mater 2015;27:5506–11.
[66] Abueidda DW, Bakir M, Abu Al-Rub RK, Bergström JS, Sobh NA, Jasiuk I. Mechanical properties of 3D printed polymeric cellular materials with triply periodic minimal surface architectures. Mater Des 2017;122:255–67.
[67] Qin Z, Jung GS, Kang MJ, Buehler MJ. The mechanics and design of a lightweight three-dimensional graphene assembly. Sci Adv 2017;3:e1601536.

[68] Liu Y, Schaedler TA, Jacobsen AJ, Lu W, Qiao Y, Chen X. Quasi-static crush behavior of hollow microtruss filled with NMF liquid. Compos Struct 2014;115:29–40.
[69] Zhou J, Deng X, Yan Y, Chen X, Liu Y. Superelasticity and reversible energy absorption of polyurethane cellular structures with sand filler. Compos Struct 2015;131:966–74.
[70] Wang L, Lau J, Thomas EL, Boyce MC. Co-continuous composite materials for stiffness, strength, and energy dissipation. Adv Mater 2011;23:1524–9.
[71] Liu Y, Wang L. Enhanced stiffness, strength and energy absorption for co-continuous composites with liquid filler. Compos Struct 2015;128:274–83.